Available online at www.sciencedirect.com

ScienceDirect

Physics Procedia 12 (2011) 21–30

Physics Procedia

LiM 2011

Effects of Radial and Tangential Polarization in Laser Material Processing

Rudolf Weber [a*], Andreas Michalowski [a], Marwan Abdou-Ahmed [a], Volkher Onuseit [a], Volker Rominger [b], Martin Kraus [a], Thomas Graf [a]

[a] *Universität Stuttgart, Institut für Strahlwerkzeuge (IFSW), Pfaffenwaldring 43, D-70569 Stuttgart*
[b] *TRUMPF Laser und Systemtechnik GmbH, Johann-Maus-Str. 2, 71254 Ditzingen, Germany*

- Invited Paper -

Short Abstract

The polarization state of a laser beam has a strong influence on the process in almost any kind of laser material processing. The benefit of material processing with cylindrical polarization was described by several authors. Recently, intra-cavity polarization generation and extra-cavity polarization conversion for industry-level high-power lasers were presented. The present paper gives an overview over the state of the art and the latest results for cutting, welding and drilling achieved at the IFSW of the University of Stuttgart.

Keywords: radial polarization; azimuthal polarization; tangential polarization; cylindrical polarization; laser cutting; laser welding; laser drilling; Fresnel absorption

1. Motivation

Laser material processing is used in a wide range of industrial applications including cutting, welding and drilling. In these processes with intensities exceeding about 10^6 W/cm^2 the absorbed laser energy creates a 3-dimensional structure such as a cutting kerf, a keyhole or an ablated surface structure. Very high aspect ratios can be achieved with actual high-brightness lasers. In each of these cases at least a part of the laser-material interaction takes place at the walls of the structure. Figure 1(a) shows a sketch of a typical geometry encountered. The beam polarization direction in the plane of interaction is called p-polarization, its orthogonal direction is s-polarization. The angle of incidence is the angle between the beam propagation direction and the surface normal. In such geometries the angle of incidence is often close to 90°.

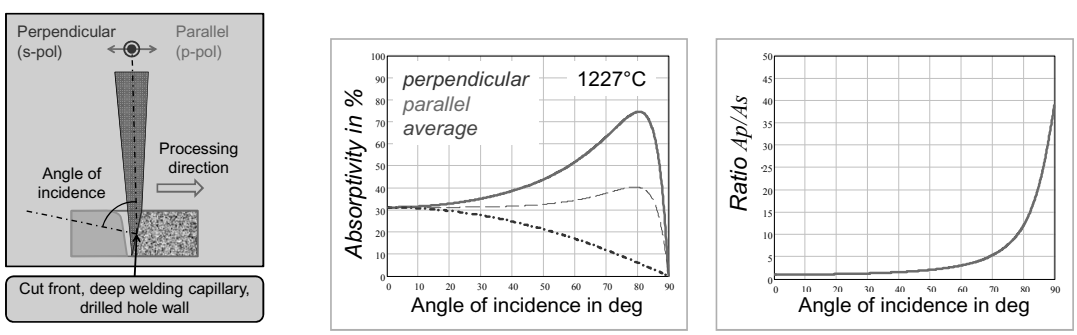

(a) (b) (c)

Figure 1. (a) Sketch of a typical laser-material interaction geometry. (b) Fresnel absorption calculated for hot iron for p- and s-polarization. (c) Ratio of the absorption of p- and s-polarization.

* Corresponding author
E-mail address: Rudolf.Weber@ifsw.uni-stuttgart.de.

doi:10.1016/j.phpro.2011.03.004

Since the work of Fresnel in the beginning of the 19th century it is known that the interaction behavior strongly depends on the polarization with respect to the plane of incidence. Figure 1(b) gives the calculated absorptivity in hot iron as a function of the angle of incidence for p and s-polarization following the theory of Fresnel.

A large difference between the absorptivity of p- and s-polarized light is seen. It is even more pronounced when plotting the ratio of the two absorptivities as shown in Figure 1(c). For angles exceeding 80° the p-absorption is more than an order of magnitude large than the s-absorption.

Figure 2 shows beam cross-sections with a schematic of polarizations states as commonly used for material processing. Up to now these polarization states were restricted to linear, circular or random. For processes as sketched in Figure 1(a) the processed surface extends along the circumference of the beam cross-section. This means that for linear polarization the laser-surface interaction either occurs in p- or in s-polarization. In the case of circular and random polarization the interaction is a time average of the p- and s-polarization state.

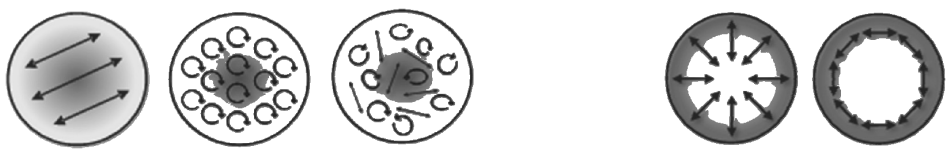

(a) (b) (c) (d) (e)

Figure 2. Laser beam cross-sections with polarization states: (a)linear (b) circular (c) random,.(d) radial, and (e) tangential

Cylindrical polarization has the two orthogonal states radial and tangential polarization as shown in Figure 2(d) and (e). The outstanding advantage of these polarization states is that the complete surface is processed with the same, temporally and spatially constant polarization state. This allows direction independent movement of the process. In addition, considering Figure 1(b) and (c) it offers the possibility of actively influencing the location of absorption by choosing the appropriate cylindrical polarization state. Furthermore, another advantageous of cylindrically polarized beams is their "doughnut-like" intensity distribution which leads to steeper slopes as compared to Gaussian distributions. This can be very well suited for materials processing since the steepness of the intensity distribution is approaching the ideal flat-top distribution but without the limitation of the depth of focusing.

In the past few years, the benefit of materials processing with cylindrical polarization was described by several authors. [1,2,3,4,5,6]. Recently, intra-cavity polarization generation and extra-cavity polarization conversion for industry-level high-power and high-brightness lasers were presented [8,9,10]. With such tools it is now possible to explore the capability and benefit of cylindrical polarization for industrial material processing. The present paper gives an overview over the theoretical background, the generation and the application of high-power cylindrically polarized beams as performed at the IFSW of the University of Stuttgart. This includes the description of cylindrically polarized laser beam generation with intra-cavity generators and extra-cavity converters, the latest results obtained with cutting, welding and drilling. The overview starts with having a closer look at the absorbed intensity distribution as can be calculated from the Fresnel equations.

2. Absorbed intensity

If light coming from a medium with index of refraction n_1 is incident to a medium with n_2 the total power decomposes into a reflected, a transmitted and an absorbed part. Here n_1 is assumed to be 1 (vacuum). For the illuminated material it is assumed that it holds $\underline{n}_2 = n_2 + ik_2$ with $k_2 > 1$ (e.g. metal) for the wavelengths of interest. In the case of a big complex part of the refraction index the optical penetration depth is given by a skin depth which is small compared to the wavelength. Therefore the transmitted part can be neglected in most cases and the absorbed laser-power leads to surface heating of the material. As a consequence the absorptivity and the reflectivity of power are connected due to the equation $A = 1 - R$. For an incoming plane wave on the surface the power-reflectivity can be described by the Fresnel-Equations

$$R_s(\Phi) = \left| \frac{\cos\Phi - \sqrt{\underline{n}_2^2 - \sin^2\Phi}}{\cos\Phi + \sqrt{\underline{n}_2^2 - \sin^2\Phi}} \right|^2 \quad \text{and} \quad R_p(\Phi) = \left| \frac{\underline{n}_2^2\cos\Phi - \sqrt{\underline{n}_2^2 - \sin^2\Phi}}{\underline{n}_2^2\cos\Phi + \sqrt{\underline{n}_2^2 - \sin^2\Phi}} \right|^2 \tag{1}$$

Here, the wave-vector of the incident and reflected wave span the plane of incidence. R_s and R_p denote the reflectivity of power for the perpendicular and parallel component of the polarization, respectively. The angle Φ is defined between the surface normal and the wave vector.

For laser-materials processing the absorbed laser beam is normally the most important source of heat for the melting and evaporation of the material. The intensity of this heat source is given by

$$A_s^{(I)}(\Phi) = A_s(\Phi)\cos\Phi = \left[1 - R_s(\Phi)\right]\cos\Phi \quad \text{and} \quad A_p^{(I)}(\Phi) = A_p(\Phi)\cos\Phi = \left[1 - R_p(\Phi)\right]\cos\Phi \,. \tag{2}$$

The additional factor $\cos\Phi$ describes the projection of the incident intensity on the tilted material surface. In the following, the index of refraction is taken to be 3.28 + i4.87. This value was measured by the authors for stainless steel at room temperature. In general the index of refraction strongly depends on temperature and material and is unfortunately not known at process relevant conditions in most cases. Nevertheless the following statements are expected to hold true also at process relevant conditions. In Figure 3 based on Eq. (2) the calculated relative absorbed intensities are shown for perpendicular and parallel polarization. It is obvious that both are monotonically decreasing functions of the incident angle. A local maximum at Brewster's angle does not exist. However, the ratio between the intensity-absorptances of the parallel and perpendicular polarization is a monotonically increasing function. It can be clearly seen that the absorbed intensity for the parallel polarized component can easily exceed the perpendicular component by a factor of >20 if the light is near to grazing incidence.

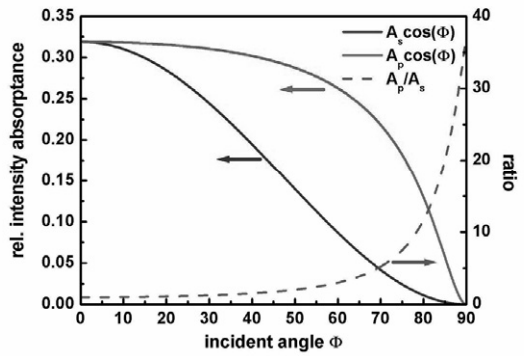

Figure 3. Relative intensity absorptance for perpendicular and parallel polarization.

This strong difference plays an important role in material-processing and will be discussed here for radially or tangentially polarized light. In addition, cylindrically polarized beams show a specific "doughnut shaped" intensity distribution as shown in Figure 4 (a) (red) in comparison with a Gaussian distribution (green).

If a radially or tangentially polarized beam is incident on a tilted plane as sketched in Figure 4 (b) the absorbed intensity strongly depends on the position within the beam profile. This is completely different compared to linearly, circularly or unpolarized light. In the example shown in Figure 4 (b) the plane of incidence is the y/z plane. Because the beams are locally linearly polarized the conditions of parallel and perpendicular incidence are fulfilled at the same time at different positions. This leads to certain "hot spots" of the absorbed intensity Figure 4 (c) on the illuminated surface which do not occur e.g. for circular polarization. Since the total absorbed power is equal for all polarizations shown (35% in this example) the absorbed intensity is locally much higher in the case of radial and tangential polarization.

For this calculation example the incident angle was chosen to be 80°, the beam diameter 200 µm (2nd moment definition), $M^2 = 2$, the index of refraction being the same as above and the wavelength was 1030 nm.

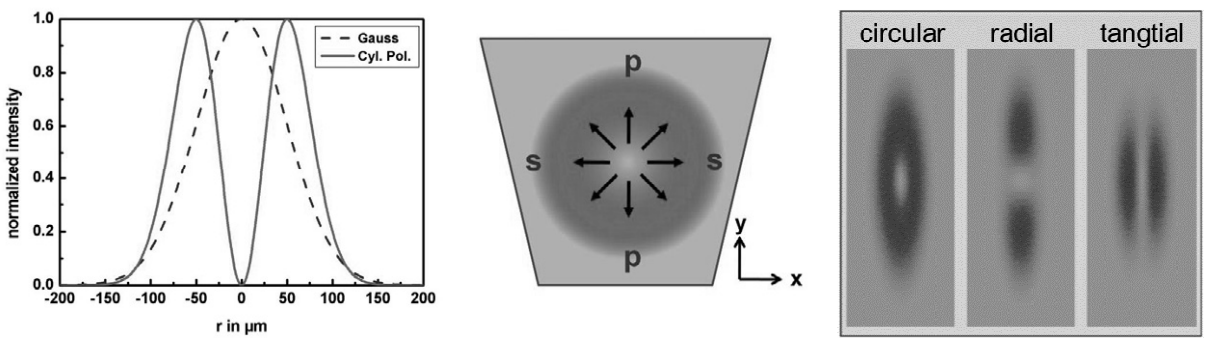

(a) (b) (c)

Figure 4. (a) Comparison of intensity distributions of cylindrically polarized (red) and Gaussian (blue dashed) beams of a radius of 100 µm. (b) A radially polarized doughnut mode is incident on a tilted plane (top-view). (c) The absorbed intensity distribution for radial and tangential polarization strongly differs from a circularly polarized beam.

The beam intensity distribution is defined by

$$I(r,z) = \frac{4 \cdot e \cdot r^2}{w(z)^2} e^{-4r^2/w(z)^2} \qquad \text{with} \qquad w(z) = w_0 \sqrt{1 + \frac{z^2}{z_0^2}}, \; z_0 = \frac{\pi w_0^2}{\lambda}. \tag{3}$$

Here w_0 and λ denote the beam waist radius and the wavelength, respectively.

From the calculations shown above the possible advantages of beams with radial or tangential polarization for materials processing (drilling, cutting, welding) are not obvious. But this is different if the illuminated object is cylindrically symmetric as well. If a beam is incident to a capillary with circular symmetry the parallel or perpendicular intensity absorption conditions are fulfilled over the whole angle.

Figure 5 shows the calculation results for an incident beam with a diameter of 60 µm which is absorbed inside a circular symmetric capillary with a diameter of 60 µm and a depth of 400 µm. It is clearly seen that the distribution of the absorbed intensity strongly depends on the polarization state.

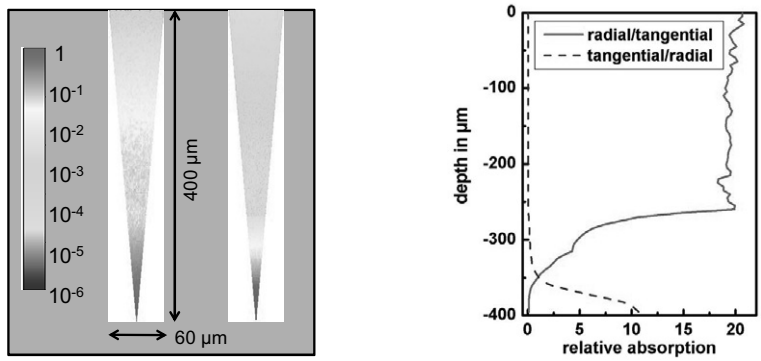

(a) (b) (c)

Figure 5. Absorbed intensity inside a capillary with circular symmetry which is illuminated by a radially (a) and tangentially (b) polarized beam. Multiple reflections are taken into account; (c) depending on polarization most of the power is absorbed in the upper part (radial) or lower part (tangential).

In this example the tangentially polarized beam allows depositing a ten times higher absorbed intensity near the tip of the capillary. This for instance leads to increased laser-drilling velocities. As the cutting and welding fronts are curved the advantages can also be observed for these processes because the angle of incidence usually exceeds about 70°.

3. Generation of cylindrically polarized beams

Cylindrical vector beams, also known as beams with axially symmetric polarization, have gained a tremendous interest in the last few years for many applications in different fields of optics, laser physics as well as in bio-medicine. This motivated several scientific groups to develop several approaches [8-28] for the generation of such beams.

In order to investigate the benefit of axially-symmetric polarization states for 1 and 10 µm wavelengths, two different approaches for the generation of beams with radial and/or tangential polarization have been developed and used at the IFSW. For the CO_2 laser system a leaky-mode polarizing grating mirror [8,9,10] was used as the end mirror of the laser cavity TruFlow 5000. The polarization control of the emitted beam relates upon the leaky waveguide modes coupling mechanism due to the presence of the grating. This induces a reduction of the reflection coefficient of the undesired polarization at the desired laser wavelength, whereas the orthogonal polarization is not or only slightly affected by the presence of the grating. Thus, by using a circular grating, as shown in Figure 6 (a), one can induce the desired reflectivity difference locally [17-20].

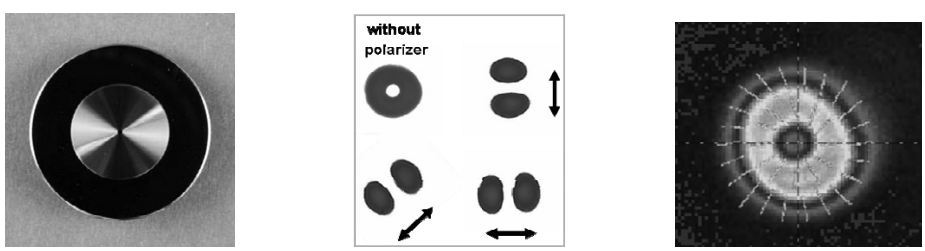

(a) (b) (c)

Figure 6. . CO_2 intra-cavity radial polarization generation. (a) Leaky mode grating mirror, (b) mode burns behind analyzer, (c) Plexiglass mode burns

In the present design, the structure parameters, i.e. the layer sequence and period and depth of the grating, were optimized to damp the tangential (corresponding to the local TE) polarization. A reflectivity difference of at least 50% (with a reflection coefficient for radial polarization of about 99.6%) between radial and tangential polarization was measured over ~300 nm spectral bandwidth at 10.6 µm. After this spectroscopic confirmation of the proper behavior of the fabricated polarizing grating mirror, the latter was introduced, as mentioned above into a TruFlow 5000. Radially polarized beams with up to 5.3 kW output power could be reached with the above described mirror. Figure 6 (b) shows the paper burn-in of the emitted beam without the analyzer (top left) and with the analyzer at different angle positions. Additionally a quantitative polarization analysis of the local polarization state over the whole beam using a custom made camera-based Stokes polarimeter [19] was performed. Figure 6 (c)

depicts the measured polarization "ellipse" over the beam cross-section. Radial polarization purity higher than 96%± 2% was measured.

In the case of solid-state lasers, namely Yb:YAG thin-disk lasers, the used and preferred solution for the material processing experiments is based on an efficient extra-cavity polarization conversion mechanism. A linear to radial/tangential polarization converter which is composed of 8 low-order half-wave segments at λ=1030 nm and which has a fixed and well-defined fast-axis orientation was used for the experimental investigations. This allows a local polarization rotation of the incident beam in the radial or tangential direction. As shown in Figure 7 (a), the switching between radial and tangential polarization can be simply and easily obtained, by a 90° rotation (relatively to the main axis (i.e. 0°) of the converter) of the polarization of the incoming beam. A photograph of the 30 mm clear aperture polarization converter used here is also shown as inset in Figure 7 (a). The complete setup including linear polarizer, beamdump and linear-to-cylindrical converter can easily be integrated into an industrial standard processing head as shown in Figure 7 (b). Up to 5.1 kW radially and or tangentially polarized laser beams were demonstrated [6]. Very recently, radially and tangentially polarized laser beams with about 8 kW of average power could be reached with a 50 mm clear aperture device [7].

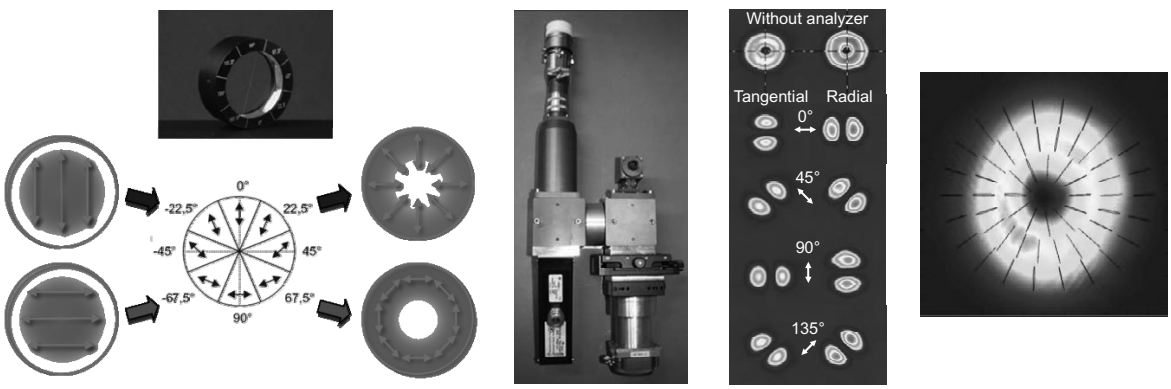

Figure 7. (a) 1 µm wavelength extra-cavity linear to circular polarization converter; (b) converter integration into an industrial standard processing head; (c) mode records behind analyzer, (d) Converter setup with fibre connector and focusing unit including beam dump.

Besides the multi-kW experiments, the converter was also used in the beam bath of a picosecond pulsed Yb:YAG thin-disk laser emitting a linearly polarized fundamental mode ($M^2 \sim 1.3$). As can be seen in Figure 7(b), cylindrical vector beams (radial and tangential polarization) with $M^2 \sim 2.5$ have been generated with a conversion efficiency measured of about 88%. Figure 7 (d) shows the the beam cross-section with the polarization measurement ellipses for 1030 nm. The polarization purity was measured in this case, after filtering and selection of the ring mode, to be 98% ± 1%.

In order to further improve the conversion efficiency of such devices, "continuous" wave plate converter systems which are based on sub-wavelength form-birefringent gratings are currently under investigation at the IFSW.

4. Cutting

Laser cutting with cylindrically polarized laser beams is for CO_2-laser cutting one of the promising possibilities to increase process efficiency and therefore the cutting velocity. In 1999 Niziev and Nesterov [1] calculated an increase of the cutting velocity up to 100% with a radially polarized CO_2-Laser in comparison to a circularly polarized laser. Since 2007 high power CO_2-Laser with radial polarization are available [9] and first cutting experiments shows an increase of cutting velocity [30].

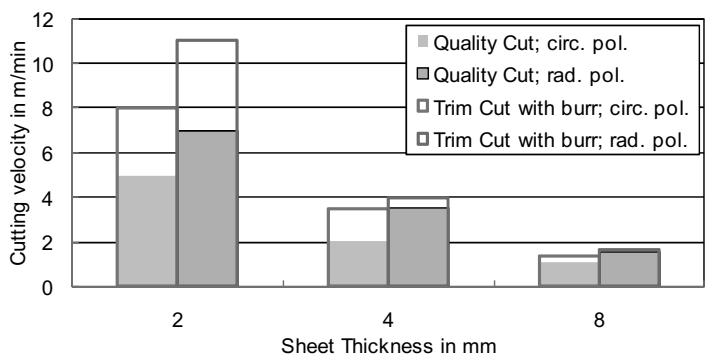

Figure 8. Cutting velocities for quality cuts and trim cuts with radial and circular polarizations.

The results achieved at the IFSW are shown in Figure 8, where the results for circularly and radially polarized cuts are compared. The columns with solid color filling show the range of quality cuts without burr formation. With circular polarizations (yellow), 5 m/min for 2 mm sheet thickness, 2 m/min for 4 mm, and 1.1 m/min for 8 mm are achieved. With radial polarization (green), the respective values are 7 m/min for 2 mm, 3.5 m/min for 4 mm and 1.5 m/min for 8 mm. This corresponds to a maximum increase of 40% at 2 mm sheet thickness. The overlaid unfilled columns show the corresponding trim cuts which allow burr formation and a low quality cutting edge. For trim cuts, the values measured for circular polarization (blue) are 8 m/min for 2 mm, 3.5 m/min for 4 mm and 1.4 m/min for 8 mm. For radial polarization (red) 11m/min for 2 mm, 4 m/min for 4 mm and 1.6 m/min for 8 mm were measured. For trim cuts, a maximum increase of cutting velocity of 37.5% resulted for 2 mm thick sheets. It can be seen that the advantage for quality cuts is higher than for trim cuts especially for sheet thicknesses greater than 2 mm. However, there is still a gap between reachable cutting velocities and the theory.

The most important factor influencing the maximum cutting speeds is the distribution of the absorbed laser power. This distribution is given by the beam intensity profile and by the local absorption coefficient which is a function of the angle between the laser beam, the surface and the local temperature. Therefore, to estimate reachable cutting velocities, it is necessary to know the real difference in the absorbed laser power between the different polarization states. One possibility to do this is to determine the process efficiency η_P. For this measurement the knowledge of the process temperature is required. One possibility to measure directly the process temperature is shown in [31]. The process efficiency is defined in Equation (3):

$$\eta_P = \frac{P_P}{P_L} = v \cdot b \cdot s \cdot \rho \cdot \left(c_P \cdot \Delta T + h_S \right) + P_V \tag{3}$$

With P_L is laser power at the work piece, v the cutting velocity, b the kerf width, s the sheet thickness, ρ the density, c_P the specific heat, ΔT the temperature difference between ambient temperature and process temperature, h_S enthalpy of fusion and P_V the losses due to heat conduction. These losses can be calculated with the approximation of Schulz et.al. [32].

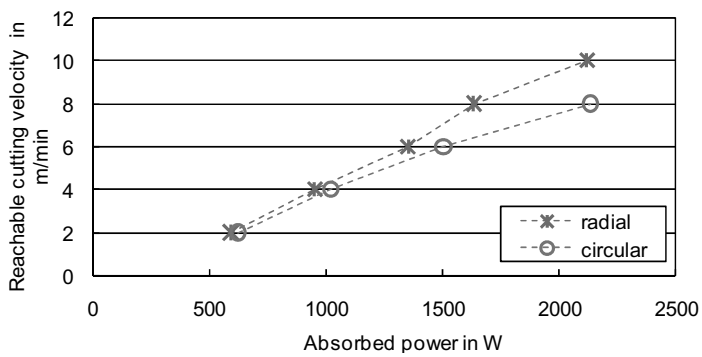

Figure 9. Attainable cutting velocities for different process efficiencies for 2mm X5CrNi18-10.

With the measured kerf width and process temperature it is possible to estimate the total absorbed power for different cutting velocities as shown in Figure 9. It can be seen, that the process efficiency as a function of the absorbed laser power is 36% higher for radial polarization than for circular.

5. Welding

Welding with high power densities can cause considerable spatter if no measures are taken to prevent it. Apart from contamination, spatter can cause a significant loss of material in the seam and therefore reduce the strength properties. The mechanisms that cause spatter are still not properly understood. The vaporization of overheated melt at the capillary front is regarded as a decisive factor in the generation of spatter, since this is the driving force behind all dynamic effects [33]. The decisive physical factor in the vaporization is the absorbed intensity. This value mainly depends on the laser wavelength and has a strong influence on the welding quality. However, welding with solid-state lasers causes more spatter on the top side than the CO_2 lasers under comparable process parameters [34,35]. Calculations have shown that the intensity distribution on the capillary front can be strongly influenced by the polarization state for solid-state lasers. These findings suggest a major impact on the welding quality [36]. Welding experiments with different polarization states at an incident laser power of 4.4 kW have shown a reduction of spattering for tangential polarization at low feed rates [7].

In order to confirm these results and to determine the laser parameter dependence for different polarization states, bead on plate welding experiments were performed on 10 mm thick mild steel S235 plates. A TruLaser 16002 with a 200 µm delivery fibre was used for the experiments. With the setup shown in Figure 7 (b) cylindrically polarized laser power of 7.9 kW was focused into a spot of 200 µm diameter. The beam parameter product of 8 mm·mrad yielded a calculated Rayleigh length of 1.25 mm. According to industrial applications the beam waist was moved 2 mm into the work piece to get the best available weld

seam quality. Since spatter behavior and weld seam quality significantly depend on the welding speed, the feed rate is varied over a wide range from 3 m/min to 18 m/min.

The degree of spatter generation was determined by process observation and visual evaluation of the work piece surface. A quantitative comparison of the amount of spatters can be obtained by determining the weight of the work piece before and after welding. The resulting weight loss is divided through the welding time required for the seam length of 125 mm.

Figure 10 (a) shows the resulting weight loss per time according to the feed rate. For all polarization conditions there is a similar curve progression observable. For small feed rates from v = 2 - 4 m/min, the weight loss per time is low with values < 50 mg/sec. In high speed recordings it can be seen that spatters mainly remove from the front and the sidewalls of the capillary within this speed range. For v ≥ 5 m/min the weight loss per time strongly increases and is attended by a change of the spatter regime. In this regime the melt is ejected from the backside of the capillary against the feeding direction. In the speed range from about v = 8 - 14 m/min a peak in the weight loss per time occurs. By rising the feed to v = 18 m/min the weight loss per time can be strongly reduced. But this high feed rate also leads to formation of humps in the subsequent melt bath, which is another undesired seam imperfection. In Figure 10 (b) the weight loss in the case of radial and tangential polarization is standardized to the conventionally used random polarization to compare the different polarizations in more details.

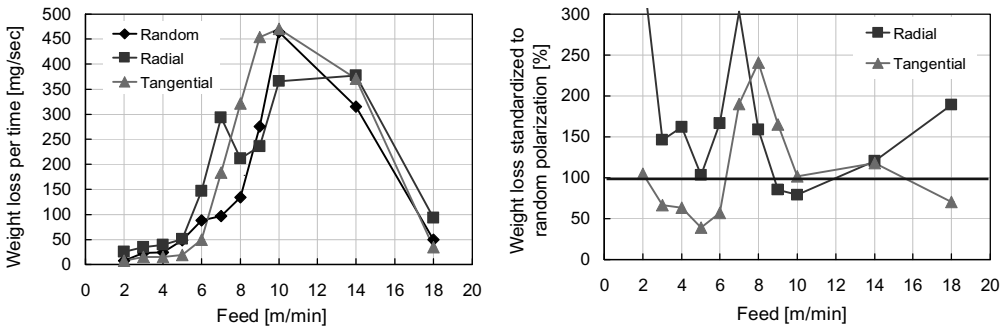

Figure 10. Weight loss per time for random, radial and tangential polarization (a) and weight loss of radial and tangential polarization standardized to random polarization (b) according to feed rate.

The resulting strong melt deficit can also be noticed by undercuts in the weld seam and a strong determination of the work piece surface due to adherent melt ejections as seen in Figure 11.

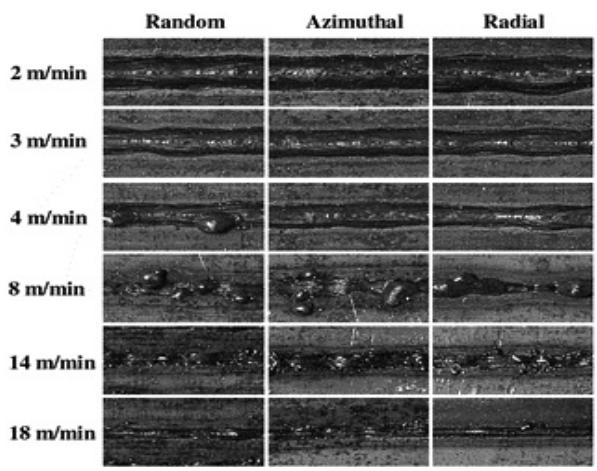

Figure 11. Surface quality for different feed rates depending on the polarization condition.

It shows that the change of polarization condition has a strong influence on the welding process. With radial polarization the weight loss by spatters even increases for low feed rates. In contrast, for v = 3 - 6 m/min, tangential polarization leads to significant weight reduction between 39% and 67%. This confirms the previous results [7]. Furthermore, the maximum feed rate for which a very high surface quality can be obtained, is increased for tangential polarization from 3 up to 4 m/min compared to the other polarization conditions. However, spatters which are ejected from the rear side of the capillary at higher welding speeds could not be prevented for the tested process parameters and focusing conditions by using cylindrical polarization.

6. Drilling

The use of ultrashort laser pulses enables the fabrication of high-precision microholes in metals without post-processing [37,38,39]. In high-aspect-ratio microdrilling, the borehole geometry is strongly influenced by the polarization of the laser beam. Ultrashort pulsed laser sources generally emit linearly polarized radiation. A linearly polarized laser beam however, is known to have different absorptivities depending on the cutting direction, as discussed above. Consequently, processing with stationary linear polarization results in linear elongation and distortion of the borehole outlet cross-section [38,39].

There are basically two ways in which round borehole geometries can be obtained, and typical circularity tolerances in the order of a few percent of the borehole diameter can be met: either utilizing axially symmetric polarization states or rotating linear polarization. The most common approach for the production of circular microholes in steel is to employ a helical drilling process together with circularly polarized radiation [39,41]. Chang et al. [40] have shown that also random-polarized radiation enables the fabrication of round borehole geometries. The use of rotating linear polarization with parallel orientation with respect to the plane of incidence can be beneficial in terms of roundness and wall smoothness at percussion drilling [38] and helical drilling in steel [39].

The first drilling experiments using radially and tangentially polarized beams were carried out on the basis of percussion drilling in steel with pulse durations in the range of a few hundred microseconds [3,10]. The linear drilling rate was reported to be higher for tangential compared to radial polarization. Moreover it was found that the boreholes manufactured with tangentially polarized radiation exhibit smaller diameters, sharper tips and higher aspect ratios. Recently, the impact of radial and tangential polarization states on ablation velocity, borehole morphology and machining quality was investigated for percussion and helical drilling in austenitic chromium-nickel steel (X5CrNi18-10) using infrared picosecond pulses [5]. The linear to radial and/or tangential polarization conversion was accomplished using a Linear to Radial/Tangential (LRA) polarization converter composed of eight half-wave plate segments [8], which was inserted into the beam delivery of a micromachining station equipped with an experimental picosecond laser system [21]. At the fundamental wavelength of 1030 nm, this laser system generates pulses with a duration of 6 ps at repetition rates of up to 206 kHz and an average output power of up to 40 W.

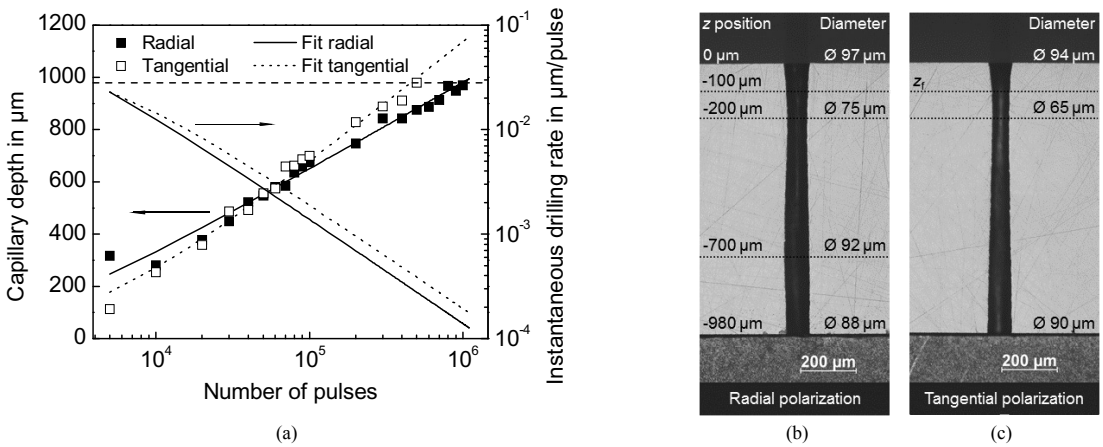

Figure 12. Microdrilling in CrNi-steel using picosecond laser pulses with radial and tangential polarization. (a) Capillary depth and instantaneous drilling rate versus number of pulses for percussion drilling with radial (■) and tangential (□) polarization. The dashed line indicates the workpiece thickness of 980 µm. (b)(c) Transverse sections of microholes in 1 mm sheets, drilled with the helical drilling technique using radially (b) and tangentially (c) polarized radiation [5].

The influence of the polarization type on the linear drilling rate at percussion drilling was investigated by fabricating holes in 980 µm sheets with pulse numbers between 10^4 and 10^6, and by subsequently determining the hole-depth. The repetition rate was 103 kHz, and the pulse energy was set to 50 µJ. The radially and tangentially polarized beams were focused 100 µm inside the material with an aberration-reduced 4-lens focusing system (f = 100 mm), which produced a focal diameter of 45 ± 3 µm according to the second moment definition. The peak energy density (power density) of the ring mode was 4.6 J/cm² ($7.7 \cdot 10^{11}$ W/cm²). Figure 12 (a) shows the results of the percussion drilling experiments. In the depicted plots of the capillary depth, the solid lines (radial polarization) and the dotted lines (tangential polarization) are logarithmic fits of the experimental data. Differentiation of the fitting functions with respect to the pulse number leads to the instantaneous drilling rate curves.

The displayed characteristics are consistent with the behavior generally observed in percussion drilling for millisecond to femtosecond pulse durations [37]. For both polarization states, the highest drilling rate (> 10^{-2} µm/pulse) is obtained at the beginning of the drilling process. A strong decrease to roundly 10^{-3} µm/pulse occurs during the first $2 \cdot 10^5$ pulses, followed by a steady decline of the drilling rate to little more than 10^{-4} µm/pulse, until eventually the penetration of the full sample thickness is completed. However, it is important to note that the behavior of the two axially symmetric polarization states differs depending on capillary depth. Whereas the drilling rate seems to be slightly higher for radial polarization during the first $7 \cdot 10^4$ pulses, which corresponds to a drilling depth of 600 µm, the tangentially polarized beam advances into the workpiece considerably faster than the radially polarized beam beyond 600 µm. As a consequence, the full sample thickness of 980 µm is penetrated after

~10^6 pulses with radial polarization, but already after ~$5 \cdot 10^5$ pulses with tangential polarization. This corresponds to a reduction of the machining time by a factor of two. The geometrical characteristics of the fabricated capillaries were each found to be similar to those obtained at microsecond drilling.

The helical drilling experiments were carried out with the same laser, focusing and material parameters as the percussion drilling experiments. Since the average laser power was only 5.15 W, a total machining time of 120 s was needed to complete the desired borehole geometry. Figure 12b shows transverse sections of two microholes fabricated with radially and tangentially polarized radiation. Despite the low pulse energy, a widened, funnel-shaped inlet is produced at both polarization states. Accordingly, the capillaries narrow to a waist located about 200 µm below the workpiece surface. Below the waist, the borehole drilled with radial polarization is barrel-shaped with the maximum diameter located at ~700 µm below the sample surface. This morphology can be explained by a high absorptivity of the radially polarized radiation, caused by parallel incidence to the walls over the entire borehole circumference and a large angle of incidence. The high absorptivity, in turn, results in extensive energy transfer to the workpiece in the sheet center and a lack of energy in the outlet zone, the latter resulting in an increasing reduction of the borehole cross-section. On the other hand, using tangential polarization, a slender capillary with straight walls and a regular conical shape, corresponding to the beam inclination angle of 3°, is produced. Since the absorptivity of the tangentially polarized radiation is comparably low at the side walls, less energy is absorbed in the upper region of the capillary, leaving a bigger fraction of the pulse energy available in the outlet zone. Reduced radial expansion and higher aspect ratios have also been observed at helical drilling with tangential polarization in 0.5 mm sheets. Regarding the machining quality of the borehole inlets and outlets, no significant difference can be stated between radial and tangential polarization. This means that, at helical drilling without drilling core in the picosecond regime, a comparable quality is achieved at parallel and perpendicular incidence of the radiation to the borehole walls.

Overall, it appears that the use of radial polarization is suitable rather for the fabrication of boreholes with relatively large diameters in thin sheets ($t \leq 500$ µm), while tangential polarization can be recommended for the generation of high aspect ratios in thick sheets ($t \geq 1$ mm) or extraordinarily small diameters ($d \leq 50$ µm).

7. Conclusion

Cylindrically polarized laser beams show a very specific absorbed intensity behavior. The findings of the calculations were confirmed by cutting, welding and drilling experiments. For these experiments, two different schemes for the generation of cylindrical polarization states were used.

For the CO_2-laser cutting experiments, a leaky mode type intra-cavity mirror was used to generate radially polarized light with power levels up to 5 kW. An increase of the cutting efficiency of up to 36 % and of the maximum cutting speed of 37.5 % was measured for 2mm stainless steel.

The experiments carried out at a wavelength of 1 µm were made with an extra-cavity linear-to-cylindrical polarization converter consisting of a segmented waveplate. Using this converter, welding experiments were performed with average power levels of up to 7.9 kW. For deep welds at low welding speeds a significant reduction of spatter behavior below 40% could be measured for tangential polarization compared to welding with random polarization.

The same converter was used for the fabrication of micro holes. These experiments were performed with a high peak power picosecond laser at the wavelength of 1 µm. The drilling efficiency was found to increase for radial polarization in case of shallow hole depths. With tangential polarization an increase in drilling efficiency was observed for deep holes. In addition, it has been shown that the hole shape differs significantly. Both findings perfectly agree with the modeling results of the absorbed intensity distributions.

In conclusion, this overview confirms the significant, positive influence of cylindrically polarized beams on the process efficiency and quality. Considering the demonstrated potential of such processing we believe that laser material processing with cylindrically polarized beams will considerably gain importance in industrial and scientific applications.

Acknowledgements

This research was supported by the Baden-Württemberg Stiftung within the project RaPoS, the Deutsche Forschungsgemeinschaft (DFG) under contract GR3172/7-1 and the German Federal Ministry for Education and Research (BMBF) under contract 13N8583.

References

[1] V. G. Niziev, A. V. Nesterov, “Influence of beam polarization on laser cutting efficiency”, J. Phys. D: Appl. Phys. 32, 1455-1461 (1999).

[2] M. Meier, V. Romano, and T. Feurer, “Material processing with pulsed radially and tangentially polarized laser radiation”, Appl. Phys. A 86, 329-334 (2007).

[3] T. Moser, M. Abdou Ahmed, M. Schäfer, A. Voss, M. Vogel, and T. Graf, “Exploiting radial polarization in material processing”, presented at the Stuttgart Laser Technology Forum, Stuttgart, Germany, 4-6 March 2008.

[4] Q. Zahn, “Trapping metallic rayleigh particles with radial polarization,” Opt. Express 12, 3377-3382 (2004).

[5] M. Kraus, M. Abdou Ahmed, A. Michalowski, A. Voss, R. Weber, and T. Graf, “Microdrilling in steel using ultrashort pulsed laser beams with radial and azimuthal polarization,” Opt. Express 18(21), 22305-22313 (2010).

[6] R. Weber, M. Abdou-Ahmed, A. Michalowski, P. Berger, P. Gärtner, V. Onuseit, M. Kraus, A. Voß, T. Graf, “Radial and azimuthal polarization in laser cutting, welding and drilling”, Advanced Laser Technologies ALT2010, Egmond-aan-Zee, Netherlands

[7] M. Abdou Ahmed et al., paper under submission

[8] M. Abdou-Ahmed, M. Vogel, V. Onuseit, A. Voss, R. Weber, and T. Graf, “Radially polarized thin-disk laser with 1-kW power,” invited talk, presented at the International Laser Physics Workshop, Barcelona, Spain, 13-17 July 2009.

[9] M. Abdou Ahmed, J. Schulz, A. Voss, O. Parriaux, J.C. Pommier, and T. Graf, “Radially polarized 3 kW beam from a CO_2 laser with an intracavity resonant grating mirror,” Opt. Lett. 32, 1824-1826 (2007).

[10] M. Abdou Ahmed, A. Voß, M. Vogel, A. Austerschulte, J. Schulz, V. Metsch, T. Moser, and T. Graf, “Radially polarized high-power lasers,” Proc. SPIE 7131, 71311I-1–71311I-10 (2008).

[11] 1M. Abdou-Ahmed, M. M. Vogel, A. Voss, and Th. Graf, "A 1-kW radially polarized thin-disk laser“, CLEO Europe 2009, Munich (2009), Germany.

[12] M. Endo, "Azimuthally polarized 1 kW CO2 laser with a triple-axicon retroreflector optical resonator“, Opt. lett. 33, 1771-1773 (2008).

[13] J. Li, K. Ueda, L. Zhong, M. Musha, A. Sihirakawa, T. Sato, "Efficient excitations of radially and azimuthally polarized Nd3+:YAG ceramic microchip laser by use of subwavelength multilayer gratings composed of Nb2O5/SiO2“, Opt. Exp. 16, 10841-10848 (2008).

[14] G. Machavariani, Y. Lumer, I. Moshe, A. Meir, and S. Jackel, "Efficient extracavity generation of radially and azimuthally polarized beams“, Opt. Lett. 32, 1468-1470 (2007).

[15] P. Phua, W. Lai, Y.Lim, B. Tan, R. Wu, K. Lai, H. Tan, "High Power Radial Polarization Conversion Using Photonic Crystal Segmented Half-Wave-Plate“, Conference on Lasers and Electro-Optics (CLEO) 2008 paper: CMO4.

[16] Siddharth Ramachandran, Poul Kristensen, and Man F. Yan, "Generation and propagation of radially polarized beams in optical fibers“, Opt. Lett. 34, 2525-2527 (2009)

[17] A. Voß, M. Abdou Ahmed, and Th. Graf, "Extension of the Jones Matrix formalism to higher-order transverse modes“, Opt. Lett. 32, N°1, 83-86, 2007.

[18] A. Voss, M. Abdou Ahmed, and Th. Graf, "Application of the extended Jones matrix formalism for higher-order transverse modes to laser resonator", Opt. Exp. 18, N°21,21540-21550, 2010.

[19] Th. Liebig, M. Abdou Ahmed, A. Voss, T. Graf, "Novel multi-sensor polarimeter for the characterization of inhomogeneously polarized laser beams", LASE, Photonics West 2010, San Francisco, California, USA. 2010.

[20] M. Abdou Ahmed, A. Voss, M. M. Vogel, and Th. Graf, "Multilayer polarizing grating mirror used for the generation of radial polarization in Yb:YAG thin-disk laser“, Opt. Lett. 32, N° 22, 3272-3274, 2007.

[21] C. Stolzenburg, and A. Giesen, “Picosecond Regenerative Yb:YAG Thin Disk Amplifier at 200 kHz Repetition Rate and 62 W Output Power”, in *Advanced Solid-State Photonics*, Technical Digest (CD) (Optical Society of America, 2007), paper MA6.

[22] T. Moser, J. Balmer, D. Delbeke, P. Muys, S. Verstuyft, and R. Baets, “Intracavity generation of radially polarized CO2 laser beams based on a simple binary dielectric diffraction grating”, Appl. Opt. 45, 8517-8522 (2006).

[23] Moshe, S. Jackel, and A. Meir, “Production of radially or azimuthally polarized beams in solid-state lasers and the elimination of thermally induced birefringence effects”, Opt. Lett. 28, 807-809 (2003).

[24] I. Moshe, S. Jackel, A. Meir, Y. Lumer, and E. Leibush, "2 kW, M2 < 10 radially polarized beams from aberration-compensated rod-based Nd: YAG lasers", Opt. Lett. 3, 47-49 (2007).

[25] S.C. Tidwell, G.H. Kim, and W.D. Kimura, “Efficient radially polarized laser beam generation with a double interferometer”, Appl. Opt. 32, 5222-5229 (1993).

[26] K. C. Toussaint, S. Park, J.E. Jureller, and N. F. Scherer, “Generation of optical vector beams with a diffractive optical element interferometer”, Opt. Lett. 30, 2846-2848 (2005).

[27] S. Quabis, R. Dorn, and G. Leuchs, “Generation of a radially polarized doughnut mode of high quality”, Appl. Phys. B 81, 597-600 (2005).

[28] W. Lai, B. Lim, P. Phua, K. Tiaw, H. Teo, and M. Hong, “Generation of radially polarized beam with a segmented spiral varying retarder,” Opt. Exp. 16, 15694-15699 (2008).

[29] Borstel,M; Erhard, S.; Schulz, J.: “Wavelength Specific Advantages of CO_2 Lasers”. In: Proceedings of SLT 2010: 8-10.6.2010.

[30] Onuseit, V; Abdou Ahmed, M.; Weber, R.; Graf, T.: “Space-resolved Spectrometric Measurements of the Cutting Front”. In: Proceedings of LIM 2011.

[31] Schulz, W.; Becker, D.; Franke, J.; Kemmerling, R.; Herzinger, G.: “Heat conduction losses in laser cutting of metals”. In: Journal of Applied Physics: 26 (1993) 1357-1363.

[32] Berger, P.; Hügel, H.; Hess, A.; Weber, R.; Graf, T.; “Understanding of Humping Based on Conservation of Volume Flow”; In: Proce. of LIM 2011

[33] V. Rominger: “Prozessuntersuchungen beim Laserstrahltiefschweißen – Festkörperlaser hoher Brillanz im Vergleich zu CO2-Lasern”, DVS Reports Vol. 267, DVS Congress 2010, Nuremberg, pp. 188-193.

[34] V. Rominger: “High-performance laser welding - A comparison of high-brilliance CO2 lasers and solid-state lasers”, Laser Technik Journal 03, (2011).

[35] Berger, P“,Absorption and Melt-Flow in Keyhole Laser Welding”. In: Proceedings of SLT 2010: 8-10.6.2010.

[36] D. Breitling, C. Föhl, F. Dausinger, T. Kononenko, and V. Konov, in *Femtosecond Technology for Technical and Medical Applications*, F. Dausinger, F. Lichtner and H. Lubatschowski, eds. (Springer, Berlin, 2004).

[37] H. Tönshoff, C. Momma, A. Ostendorf, S. Nolte, and G. Kamlage, “Microdrilling of metals with ultrashort laser pulses,” J. Laser Appl. 12, 23-27 (2000).

[38] Föhl, C., Dausinger, F., “High precision deep drilling with ultrashort pulses” Proc. SPIE 5063, 346-351 (2003).

[39] J. Chang, B. Warner, E. Dragon, and M. Martinez, “Precision micromachining with pulsed green lasers”, J. Laser Applications 10, 285-291 (1998).

[40] Ancona, F. Röser, K. Rademaker, J. Limpert, S. Nolte, and A. Tünnermann, “High speed laser drilling of metals using a high repetition rate, high average power ultrafast fiber CPA system”, Opt. Express 16, 8958-8968 (2008).

[41] M. Kraus, S. Collmer, S. Sommer, and F. Dausinger, “Microdrilling in steel with frequency-doubled ultrashort pulsed laser radiation”, J. Laser Micro/Nanoengineering 3, 129-134 (2008).

[42] Michalowski, D. Walter, F. Dausinger, and T. Graf, “Melt dynamics and hole formation during drilling with ultrashort pulses”, J. Laser Micro/Nanoengineering 3, 211-215 (2008).